

The Infrared to Gamma-Ray Pulse Shape of the Crab Nebula Pulsar

Stephen S. Eikenberry and Giovanni G. Fazio

Harvard-Smithsonian Center for Astrophysics, Cambridge, MA 02138

Received _____; accepted _____

arXiv:astro-ph/9607120v1 23 Jul 1996

ABSTRACT

We analyze the pulse shape of the Crab Nebula pulsar in the near-infrared, optical, ultraviolet, X-ray, and gamma-ray bands, including previously unpublished ROSAT HRI observations. We show that, in addition to the previously known trend for the fluences of the Bridge and Peak 2 to increase with energy relative to the fluence of Peak 1, there is a small but statistically significant trend for both to decrease with energy relative to Peak 1 over the near-infrared range. We find that the phase separation between the two peaks of the pulse profile decreases nearly continuously as a function of energy over 7 decades of energy. We show that the peaks' full-width half-maxima are significantly variable over this energy range, but without any clear pattern to the variability. We find that the differences between the energy dependences of the leading and trailing edge half-width half-maxima of both peaks found by Eikenberry *et al.* (1996a) also continue over 7 decades of energy. We show that the cusped shape of Peak 2 reverses direction between the infrared/optical and X-ray/gamma-ray bands, while the cusped shape of Peak 1 shows weak evidence of reversing direction between the X-ray and gamma-ray bands. Finally, we find that many of the pulse shape parameters show maxima or minima at energies of 0.5-1 eV, implying that an important change in the pulsar emission is occurring near this energy. Many of these complex phenomena are not predicted by current pulsar emission models, and offer new challenges for the development of such models.

Subject headings: pulsar: individual (PSR0531+21) - radiation mechanisms: non-thermal - stars: neutron

1. Introduction

The Crab Nebula pulsar is one of the best-studied objects in astrophysics. In the almost 30 years since its discovery, it has been observed in almost every waveband, and has been particularly important to understanding the nature of pulsars and their emission mechanisms. One of the measurements of key interest is the the shape of the pulse profile. The double-peaked appearance, the sharpness of the peaks¹, and their separation by 0.4 in phase (see Figure 1) are among the leading motivators of many of the theories attempting to explain the pulsar emission mechanism (i.e. Cheng et al., 1986a,b; Chiang and Romani, 1994; Romani and Yadigoraglu, 1995; Daugherty and Harding, 1996 - hereafter CHRa,b; CR94; YR95; DH96, respectively). In these models of Crab Nebula pulsar emissions, primary energy generation occurs in particle accelerator “gaps” in the magnetosphere. The accelerated particles produce γ -rays through curvature radiation, and these γ -rays interact with the magnetosphere in a complex manner to produce the X-ray, ultraviolet (UV), optical, and infrared (IR) pulsations, so that the non-radio emissions are closely linked to each other².

Recent work by the authors and their collaborators (Eikenberry *et al.*, 1996a,b) has revealed energy dependences in the pulse shape over the IR to UV range, some of which are

¹We refer to the 2 major features in the profile as Peak 1 and Peak 2, joined by the Bridge. This is to avoid confusion, as some previous authors refer to the Bridge as the “Interpulse”, while others use that name for Peak 2.

²While some of the radio emission is thought to be linked with the higher energy emissions, it may originate elsewhere in the magnetosphere. As an example, the recent work of Moffett and Hankins (1996) shows that Peak 1 and Peak 2 are not identifiable features over much of the radio frequency range. For this reason, we exclude the radio pulse shape from our analyses here.

challenging the current pulsar emission models. In particular, the half-widths of both peaks show different energy dependences from their leading to trailing edges, a phenomenon which is not predicted by any of the emission models. In this context, we are presenting new analyses of the Crab Nebula pulsar’s pulse shape from the IR to γ -ray bands. We are using new pulse profiles in the IR and X-ray bands with previously unavailable signal-to-noise. We pay particular attention to the peak leading and trailing edge half-widths, which, as mentioned above, are providing new challenges for the theoretical models. Also, in contrast to previous work on this subject (e.g. Ramanamurthy, 1994), we treat all the pulse profiles with uniform analysis techniques to prevent potential bias from differences in treatment. Thus, we hope that such an analysis of the pulse shape over 7 decades in energy will provide new insights into the nature of the pulsar emission mechanism.

2. Data

2.1. X-ray pulse profile

We created the X-ray pulse profile for the Crab Nebula pulsar from a series of archival ROSAT High-Resolution Imager (HRI) sequences originally obtained on September 2-3, 1992 (MJD 48881 and 48882). We downloaded 8 such sequences from the HEASARC data archive and performed the preliminary analyses using the PROS software package. First, we created images of the individual observations, which revealed the pulsar as a bright point source superposed on an extended synchrotron nebula. Second, for each sequence we extracted all photon events in an aperture with 40 arcsecond diameter centered on the point source, selecting a total of $\sim 954,000$ events over the $\sim 24,000$ s total integration time. Third, we corrected the photon arrival times to the solar system barycenter, and in order to check the X-ray timing, we epoch-folded each sequence over a range of periods with an assumed period derivative of $\dot{P} = 4.20918 \times 10^{-13}$ s/s and determined the period

which maximized the χ^2 -value for the pulse profile. In all 8 sequences, the measured period matched that predicted from the Jodrell Bank radio timing ephemeris (R. Pritchard, private communication) within statistical uncertainties (typically 0.5 to 5 nanoseconds), with $P_0 = 0.0334083300s$ and $\dot{P} = 4.20918 \times 10^{-13}s/s$ at MJD 48880.00 . Concluding that this verifies the validity of the X-ray timing, we then folded each sequence at the period and period derivative given by the Jodrell Bank ephemeris into pulse profiles with 512 phase bins, for a time resolution of $65.3\mu s$. Finally, we corrected the profiles for deadtime effects, combined all 8 pulse profiles in phase and subtracted the background, resulting in the X-ray pulse profile shown in Figure 1. This is the highest signal-to-noise X-ray pulse profile of the Crab Nebula pulsar obtained to date.

2.2. Other pulse profiles

We selected the remaining pulse profiles from a variety of sources. For the γ -ray band, we chose the OSSE pulse profile (Ulmer *et al.*, 1994) from the Compton Gamma-Ray Observatory (CGRO) for its combination of energy coverage and high signal-to-noise. (We do not include data from higher energy ranges, such as those provided by the EGRET instrument on CGRO due to the lower signal-to-noise available at these energies). The UV and optical pulse profiles come from Hubble Space Telescope High-Speed Photometer observations of the Crab Nebula pulsar (Percival *et al.*, 1993), while the near-infrared pulse profiles were obtained by the authors and their collaborators using the Solid-State Photomultiplier (SSPM) instrument on the Multiple Mirror Telescope (Eikenberry *et al.*, 1996a,b). We present a summary of the energy (and, where sensible, wavelength) coverage of the pulse profiles in Table 1.

3. Analysis - Overall pulse shape

The overall similarities and differences in the pulse shape over a broad energy range from energies of ~ 1 eV to $\sim 10^6$ eV have been known for some time, and may be clearly seen in the typical pulse profiles we present in Figure 2. All the pulse profiles in this range show 2 peaks occurring at the same phase, joined by a lower (but non-zero) flux “Bridge”. On the other hand, we can clearly see in Figure 2 that the integrated flux (or fluence) of Peak 2 increases relative to Peak 1 with energy, as does the fluence of the Bridge. We plot the fluence ratios of the Bridge versus Peak 1 and Peak 2 versus Peak 1 in Figure 3, again clearly showing the overall trend for an increase in both ratios with energy. However, we note that there is also a small but statistically significant trend for both fluence ratios to decrease with energy at energies below 1 eV. Inspection of higher energy profiles reveals that the fluence ratios also decrease at energies greater than ~ 1 MeV (Ulmer *et al.*, 1994). Another feature that begins to appear with the high signal-to-noise of the pulse profiles in Figure 2, but has been previously unnoticed, is the shape reversal of Peak 2 - from a fast rise and slow fall in the IR/optical range, to a slow rise and fast fall in the X-ray/ γ -ray range. We will return to this effect and present quantitative evidence of its existence below.

4. Analysis - Detailed pulse shape

Given the overall picture of the evolution of pulse shape with energy, we now turn to more detailed, quantitative analyses. First, we measure the phase separation between the 2 peaks and the full-width half-maxima (FWHM) of the 2 peaks versus energy. We then move on to the analysis of the peaks’ half-width half-maxima (HWHM) versus energy, and any differences between the leading and trailing edge HWHM. Finally, we analyze a new shape factor for evidence of peak shape reversal as a function of energy.

4.1. Peak-to-peak phase separation

Percival *et al.* (1993) were among the first to show that the phase separation between Peak 1 and Peak 2 changes with energy, and since then many authors have measured this effect in an attempt to understand its relation to and impact on the emission mechanism (i.e. Ransom *et al.* 1994; Ramanamurthy, 1994; Ulmer *et al.*, 1994). However, the techniques used to measure the phase separation have varied from author to author and from energy band to energy band, occasionally resulting in method-dependent biases (see Eikenberry *et al.*, 1996b for further discussion).

Here, we present a measurement of the peak-to-peak phase separation as a function of energy using the same techniques in all energy bands. First, we fit the central regions of each peak with a 6th-order polynomial, and take the peak position to be at the maximum of the fit. The phase separation is then simply the difference in phase between the 2 maxima. In order to estimate the uncertainties in this technique, we perform a Monte Carlo simulation as follows. First, we take the phase bins near the peak region and assume that the noise in the number of counts in each bin follows a Poisson distribution. Next, we take the fit to the central region of the peak and add to each bin a normally-distributed random number with a variance corresponding to the Poisson noise for that bin. We fit this new profile and measure the new phase separation, and then repeat the procedure 1000 times for each energy band and peak. Finally, we take the standard deviation of the simulated separations to be the 1σ uncertainty in the measured value. The resulting separations and their uncertainties are presented in Figure 4 and Table 2.

The peak-to-peak phase separation appears to be a more or less smooth function of energy from IR to γ -ray energies. The separation decreases with energy over the range from 0.9 eV to 10^6 eV. However, there is some evidence of a turnover or break in this trend at $E = 0.7$ eV ($\lambda = 1.65\mu\text{m}$). While, Ulmer *et al.* (1994) have shown that the peak-to-peak

separation shows no change with energy over the range ~ 50 keV to ~ 500 keV, their uncertainties of ~ 0.01 in phase are large enough to hide the effects that we see here.

4.2. Full-width half-maxima

The peak full-width half-maxima (FWHM) are easily measured even in relatively low signal-to-noise pulse profiles (such as in γ -ray observations), are related to the geometry of the emission mechanism, and are thus often among the key predicted parameters in pulsar emission models (e.g. Ho (1993)). We measure the FWHM of the 2 peaks from the phase difference between the points where the profile reaches 1/2 of the peak maximum value. In order to determine the uncertainties in the FWHM, we perform the following Monte Carlo simulation. First, we fit independent third-order polynomials to the leading and trailing edges of the peaks, and then measure the FWHM from the points where the fit equals one-half of the peak maximum (in all cases, the fit determination matches the original measurement). Second, we take the fitted counts per bin and add a normally-distributed random number with a variance corresponding to the Poisson noise for that bin. We then make fits and determine the FWHM for these new profiles. We repeat this procedure 1000 times for each peak, and we take the 1σ uncertainty in the FWHM to be the standard deviation in the Monte Carlo FWHM distribution.

We present the resulting FWHM values and their uncertainties in Figure 5 and Table 2. The Peak 1 FWHM shows significant variability from one data point to the next over much of the energy range, but without any clear pattern. The Peak 2 FWHM is also variable over the IR to γ -ray energy range, and appears to show a trend for larger FWHM at lower energies. However, given the known differences in the energy dependences of the HWHM values that make up the FWHM (Eikenberry *et al.*, 1996a), the informational value of the FWHM measurements is unclear.

4.3. Half-width half-maxima

In previous work, we and our collaborators have found differences in the energy dependences of the peak half-widths for the leading and trailing edges of the IR-UV pulse profile peaks of the Crab Nebula pulsar (Eikenberry *et al.*, 1996a,b). We perform similar analyses here to investigate whether such differences are consistently present across this larger energy range and to determine their form over this range. We measure the half-widths as the phase difference between the peak maximum and the points where the profile drops to 1/2 of the peak maximum value. We then perform Monte Carlo simulations, identical to those used for the FWHM analysis, to determine the uncertainties in the half-width half-maxima (HWHM). We present the resulting HWHM measurements and their uncertainties in Figures 6 and 7 and in Table 2.

The HWHM results show a range of interesting characteristics in their energy dependences. First, we note that in both peaks the HWHM energy dependences of the leading edges differ from the trailing edges, and the leading and trailing edge energy dependences also differ from Peak 1 to Peak 2. Second, we note that the difference between leading and trailing edge HWHM energy dependence is clearly visible in Peak 1 for the X-ray and γ -ray data points alone, confirming that these differences do indeed persist over the entire energy range. Finally, we examine the particular shapes of the energy dependences for the individual half-widths. In Figure 6(a), we see that the Peak 1 leading edge half-width shows a distinct maximum in the IR at $E=0.9$ eV, which is either a peak in a smooth curve from 0.5 eV to 10^6 eV, or a break between 2 curves covering this range. The Peak 1 trailing edge HWHM (Figure 6(b)), on the other hand, shows a minimum in the UV (5.4 eV). Again, this may either be part of a smooth curve over the energy range, or evidence of a break between two curves. In Figure 7(a), the Peak 2 leading edge half-width shows an apparently flat energy dependence over the IR to γ -ray range, but with several

data points showing significant deviations from the average value. The Peak 2 trailing edge half-width (Figure 7(b)) shows a very similar energy dependence to the Peak 1 leading edge half-width, with a maximum at $E=0.9$ eV.

4.4. Peak cusping factor

As noted earlier, we see in Figure 2 evidence of a reversal in the cusped shape of Peak 2, from a short rise and long fall in the IR profile, to a long rise and short fall in the X-ray and γ -ray bands. In order to quantify this behavior, we introduce a new parameter which we call the "peak cusping factor". The peak cusping factor (PCF) is defined to be the logarithm of the ratio of the leading edge half-width to the trailing edge half-width, or

$$PCF = \log_{10} \frac{HWHM(lead)}{HWHM(trail)}. \quad (1)$$

As can be seen, a change in sign in the PCF means a reversal in the relative steepness of the leading and trailing slopes of the peak - from a faster rise than fall to a faster fall than rise, or vice versa. We present the PCFs for Peaks 1 and 2 in Figure 8 and Table 2. The Peak 1 PCF appears to be constant from 0.75 eV to 5.4 eV, with a significantly lower value at 0.5 eV and an apparently continuous decline from 5.4 eV to 10^6 eV. Note that all of the values are positive, except for the γ -ray data point. However, this point lies only $\sim 1.2\sigma$ below 0, and thus fails to provide convincing evidence of a shape reversal in Peak 1. On the other hand, such a reversal is clearly evident in the Peak 2 PCF (see Figures 8 and 9). The IR-UV data points are all below 0 or consistent with negative values, while the X-ray and γ -ray data points are clearly positive. Thus we see that even some of the large-scale properties of the "canonical" Crab Nebula pulsar pulse shape, such as a faster rise than fall in Peak 2, are in fact energy-dependent.

5. Discussion

5.1. Pulsar emission models

We begin our discussion with a brief review of the pertinent aspects of the pulsar emission models for the Crab Nebula pulsar, as they provide a theoretical framework for considering the results we present above. One of the leading models is the 2-gap outer gap model, proposed by Cheng, Ho, and Ruderman (CHRa,b). In this model, particles are accelerated in a magnetospheric vacuum gap near the light cylinder, beaming radiation tangent to the magnetic field direction through inverse Compton (at γ -ray energies) and synchrotron (at lower energies) processes. The 2 peaks of the pulse profile arise from 2 separate gaps, each corresponding to a pulsar magnetic pole, with the separation of 0.4 in phase resulting from the time-of-flight delay between the 2 gaps along the observer's line of sight. Relativistic aberration distorts the magnetic field geometry from that of a simple dipole in the observer's rest frame, allowing variable time-of-flight delays from adjacent field lines, so that the photons from separate regions may arrive at the observer at the same time. Thus, the sharpness of the peaks arises from a caustic in the observed phase, where the emission from a large number of physical regions within the gap reach the observer at the same observed phase.

A recent variant of this model is the 1-gap outer gap model proposed by Chiang and Romani (1994) and Romani and Yadigoraglu (1995). In this model, the gap extends azimuthally completely around the pulsar, while the 2-gap model assumes that the gaps have some limited azimuthal extent. The emission process is fundamentally the same as in the 2-gap model, but detailed calculations by Chiang and Romani (1994) show that a single gap unlimited in azimuth will produce 2 caustics, and thus 2 peaks in the pulse profile. Thus the observed emission arises from only one gap and one magnetic pole.

Finally, we consider a different class of model - the polar cap (PC) gap models, specifically in the form proposed by Daugherty and Harding (1996). In the PC model, particles are accelerated in a vacuum gap and emit the observed radiation tangent to the magnetic field lines through inverse Compton and synchrotron processes (as with the outer gap models), but in a region just above the pulsar’s magnetic pole(s). Here, far from the light cylinder, relativistic aberration plays a much smaller role, and the observed pulse shape largely arises from variations in the particle distribution across the magnetic field lines.

5.2. Overall pulse shape

As noted above, our results confirm the overall trend for the fluence of Bridge and Peak 2 to increase relative to Peak 1 with energy. However, the fluence ratios for both the Bridge and Peak 2 versus Peak 1 show a decrease with energy below 1 eV. Similarly, when Ulmer *et al.* (1994) subdivide the γ -ray profiles into smaller energy bands, they find that the ratio of the Bridge + Peak 2 to Peak 1 clearly decreases over the range from a few hundred keV to a few MeV. Thus, while the overall trend holds, there appear to be turnovers at both the high and low ends of the energy range.

The overall trend for the increase with energy of the Bridge and Peak 2 relative to Peak 1 has differing implications for each of the models above. In the 2-gap outer gap model, we have different viewing angles to the 2 gaps, with a more ”head-on” view of the gap producing Peak 1. Furthermore, the gap is subdivided into 2-3 emitting regions, each of which has different typical energies (i.e. γ -ray, X-ray, optical/infrared), different beaming directions, and different opening angles. Thus different viewing angles provide different combinations of the emissions from the various regions, giving different overall spectra. Therefore, the difference in viewing angle between Peak 1 and Peak 2 may explain the

observed rise of Peak 2 with energy relative to Peak 1. However, the 2-gap outer gap models offer no explanation for the existence of the Bridge at all, let alone its energy dependence. Kamae and Sekimoto (1995) have proposed a composite model which may remedy this situation, with the 2-gap outer gap producing Peak 1 and Peak 2, while the Bridge emission arises from a PC gap. In the 1-gap outer gap model, the unlimited azimuthal extent of the gap creates Bridge emission between the 2 peaks (CR94), but no predictions of the energy dependence of the pulse shape have been made to date. In Polar Cap models, a hollow cone geometry for the particle distribution can also reproduce a Crab-like pulse shape. While the PC models do not give explicit predictions for the pulse shape as a function of energy, the symmetry of the current models (DH96) does not seem to allow significant differences between Peak 1 and Peak 2 as we observe here.

5.3. Peak-to-peak phase separation

As noted above, the phase separation between Peak 1 and Peak 2 shows an apparently continuous trend to decrease with energy over much of the IR to γ -ray energy range. With the detailed coverage here though, we can see that this trend is not a linear or even constant-power-law function of energy, as has been previously considered (e.g. Ramanamurthy, 1994). Nevertheless, this effect again seems to arise naturally in the 2-gap outer gap model. In this model, the gap is "stratified" in energy, so that the lower energy radiation emanates from a region further from the neutron star than the higher energy radiation. Thus, lower energy emissions from the 2 different gaps will have larger physical separations between them, giving greater time-of-flight delays to the observer, and hence greater phase separations.

It is not clear from the current 1-gap outer gap models whether or not the predicted phase separation should decrease with energy. However, energy stratification in the

hollow-cone emitting region of the PC model similar to that of the 2-gap outer gap model may also produce a decrease in phase separation with energy.

5.4. Peak widths (FWHM and HWHM)

While the peak FWHM values show significant variability with energy over the IR to γ -ray energy range, no clear pattern for this variability is evident. This is not particularly surprising given that the FWHM is composed of the leading and trailing edge HWHM, and, as seen above, the HWHM energy dependences change from leading to trailing edges. Thus, we conclude only that the peak FWHM measurements, despite their common appearance in the scientific literature, are of dubious informational value.

The HWHM analyses clearly show that the energy dependences of the HWHM differ between the leading and trailing edges of the individual peaks, confirming our earlier work in the IR-UV range (Eikenberry *et al.*, 1996a). Furthermore, the HWHM are apparently continuous functions of energy over most, if not all, of the energy range from $\sim 0.5 - 10^7$ eV. The possible exceptions to this continuous behavior are the apparent breaks (or, alternatively, maxima and minima) evident in the IR to UV ranges of the Peak 1 leading and trailing edge HWHM and the Peak 2 trailing edge HWHM. This behavior may be indicative of an important change in the pulsar emissions in the IR to UV range, though the exact nature of this change is not currently clear. Finally, as in Eikenberry *et al.* (1996a), we note that none of these differences in the energy dependences of the HWHM are predicted by current pulsar emission models.

5.5. Peak 2 shape reversal

The most exciting new energy-dependent characteristic of the pulse profile that we have found is the shape reversal of Peak 2. As can be seen in Figure 9, Peak 2 shows a fast rise and slow fall in the IR-optical range, but a slow rise and fast fall in the X-ray and γ -ray range. This work represents the first clear evidence of such a reversal. As with the HWHM energy dependence, this behavior is not predicted by any current models, and offers a significant challenge for the development of future models. The shape reversal of Peak 2 with energy also confirms the significant energy dependence of the Crab Nebula pulsar’s pulse shape.

5.6. The importance of the lower energy emissions

Another new feature also appears in many of the analyses presented here: the presence of maxima or minima of many of the pulse shape parameters in the near-infrared energy range (0.5-1 eV). The ratio of the Bridge fluence to the Peak 1 fluence (Fig. 3a), the ratio of the Peak 2 fluence to the Peak 1 fluence (Fig. 3b), the peak-to-peak phase separation (Fig. 4), the Peak 1 leading edge HWHM (Figure 6a), the Peak 2 trailing edge HWHM (Figure 7b), and the Peak 2 peak cusping factor (Fig. 8b) all show such behavior. The fact that so many of the pulse shape parameters show maxima or minima at 0.5-1 eV seems to imply that an important change in the pulsar emission is occurring near this energy.

6. Conclusion

We have collected pulse profiles of the Crab Nebula pulsar in the near-infrared, optical, ultraviolet, X-ray, and γ -ray energy bands, including previously unpublished high signal-to-noise X-ray observations with the ROSAT High-Resolution Imager (HRI) with

65.3 μ s time resolution. For the first time, the pulse shape over such a broad energy range has been subjected to uniform analysis techniques, and we present the conclusions from these analyses below:

1) The overall pulse shape consists of 2 large Peaks joined by a non-zero Bridge of emission. The ratios of the fluences of the Bridge and Peak 2 relative to Peak 1 show an overall trend to increase with energy. While this behavior can be explained in the outer gap emission model, the symmetry of the current polar cap model may not allow such variations. Furthermore, the analyses here show that the overall trend reverses at low energies (< 1 eV), while Ulmer *et al.* (1994) have shown that the trend also reverses at high energies (> 1 MeV).

2) The peak-to-peak phase separation shows a non-linear trend to decrease with energy over much of the range. This trend is consistent with energy stratification of the emission region in both outer gap and polar cap emission models.

3) The peaks' full-width half-maxima (FWHM) show significant variability over the infrared to γ -ray energy range, but with no definite trend or pattern. However, such behavior matches expectations given the known differences in the energy dependences of the peaks' leading and trailing half-widths.

4) The energy dependences of the peaks' half-width half-maxima (HWHM) differ between the leading and trailing edges of the individual peaks, confirming our earlier work in the IR-UV range (Eikenberry *et al.*, 1996a). Furthermore, the HWHM are apparently continuous functions of energy over most of the energy range, with possible exceptions to this continuous behavior being the apparent breaks (or, alternatively, maxima and minima) evident in the IR to UV ranges. These differences in the energy dependences of the HWHM are not predicted by current pulsar emission models.

5) The cusped shape of Peak 2 appears to reverse itself, showing a fast rise and slow fall in the IR-optical range, but a slow rise and fast fall in the X-ray and γ -ray range. This work represents the first clear evidence of such a reversal. As with the HWHM energy dependence, this behavior is not predicted by any current models, and offers a significant challenge for the development of future models. The shape reversal of Peak 2 with energy also confirms the significant energy dependence of the Crab Nebula pulsar's pulse shape.

6) Many of the pulse shape parameters show maxima or minima at energies of 0.5-1 eV, implying that an important change in the pulsar emission is occurring near this energy.

7) Many of the complex phenomena we report here are not predicted by current pulsar emission models, and offer new challenges for the development of such models.

We would like to thank M. Ulmer for providing the OSSE pulse profile; J. Dolan and the HST HSP team for providing the optical and UV pulse profiles; F. Seward and the SAO PROS support group for help with the ROSAT data reduction; R. Pritchard for supplying the Jodrell Bank Crab timing ephemeris in advance of publication; Team SSPM (S. Ransom, J. Middleditch, J. Kristian, and C. Pennypacker) for support of the IR research, and Rockwell International (K. Hays, M. Stapelbroek, R. Florence) for providing the SSPM. S. Eikenberry is supported by a NASA Graduate Student Researcher Program fellowship through NASA Ames Research Center.

REFERENCES

- Cheng, K.S., Ho C., and Ruderman, M. 1986a, ApJ, 300, 500
- Cheng, K.S., Ho C., and Ruderman, M. 1986b, ApJ, 300, 500
- Chiang, J. and Romani, R.W. 1994, ApJ, 436, 754
- Eikenberry, S.S., Fazio, G.G., Ransom, S.M., Middleditch, J., Kristian, J., Pennypacker, C.R., 1996a, ApJ Letters, in press.
- Eikenberry, S.S., Fazio, G.G., Ransom, S.M., Middleditch, J., Kristian, J., Pennypacker, C.R., 1996b, ApJ, submitted.
- Daugherty, J.K. and Harding, A.K. 1996, ApJ, 458, 278
- Ho, C. 1993, in *Isolated Pulsars*, (Cambridge University Press), Van Riper, Epstein, and Ho (eds), p.271
- Kamae, T. and Sekimoto, Y. 1995, ApJ, 443, 780
- Moffett, D.A. and Hankins, T.H. 1996, ApJ, submitted
- Percival, J.W., Biggs, J.D., Dolan, J.F., Robinson, E.L., Taylor, M.J., Bless, R.C., Elliot, J.L., Nelson, M.J., Ramseyer, T.F., van Citters, G.W. 1993, ApJ, 407, 276
- Ramanamurthy, P.V. 1994, A&A, 284, L13
- Ransom, S.M., Fazio, G.G., Eikenberry, S.S., Middleditch, J., Kristian, J.A., Pennypacker, C.R. and Hays, K.M. 1994, ApJ, 431, L43
- Romani, R.W. and Yadigaroglu, I.-A. 1995, ApJ, 438, 314
- Ulmer, M.P., Lomatch, S., Matz, S.M., Grabelsky, D.A., Purcell, W.R., Grove, J.E., Johnson, W.N., Kinzer, R.L., Kurfess, J.D., Strickman, M.S., Cameron, R.A., Jung, G.V. 1994, ApJ, 432, 228

Table 1. Pulse Profile Energy Coverage

Band	Energy Range	Wavelength Range (μm)
K	0.47–0.56 eV	2.00–2.40
H	0.63–0.74 eV	1.51–1.79
J	0.81–0.99 eV	1.11–1.39
V	1.6–2.8 eV	0.4–0.7
UV	3.9–6.6 eV	0.17–0.29
X-ray	0.2–2 keV	...
γ -ray	0.05–10 MeV	...

Table 2. Pulse Shape Analysis Results

Parameter ^a	Energy Band						
	γ -ray	X-ray	UV	V	J	H	K
Peak-to-peak separation	0.398	0.402	0.4045	0.4057	0.4069	0.4099	0.4087
	± 0.003	± 0.002	± 0.0015	± 0.0003	± 0.0005	± 0.0005	± 0.0003
Peak 1 FWHM	0.041	0.0424	0.0391	0.04363	0.0489	0.0444	0.0486
	± 0.005	± 0.0010	± 0.0006	± 0.00012	± 0.0005	± 0.0010	± 0.0005
Peak 2 FWHM	0.070	0.076	0.073	0.0815	0.091	0.087	0.086
	± 0.005	± 0.003	± 0.003	± 0.0008	± 0.003	± 0.005	± 0.004
Peak 1 HWHM (lead)	0.016	0.0252	0.0274	0.0302	0.0339	0.0298	0.0270
	± 0.004	± 0.0018	± 0.0013	± 0.0006	± 0.0010	± 0.0013	± 0.0010
Peak 1 HWHM (trail)	0.024	0.018	0.0117	0.0135	0.0151	0.0146	0.0215
	± 0.004	± 0.002	± 0.0012	± 0.0006	± 0.0009	± 0.0013	± 0.0010
Peak 2 HWHM (lead)	0.043	0.051	0.037	0.0376	0.0323	0.039	0.037
	± 0.012	± 0.003	± 0.003	± 0.0007	± 0.0016	± 0.005	± 0.004
Peak 2 HWHM (trail)	0.023	0.025	0.034	0.0439	0.059	0.045	0.048
	± 0.004	± 0.003	± 0.004	± 0.0008	± 0.002	± 0.007	± 0.005
Peak 1 PCF ^b	-0.18	0.15	0.39	0.35	0.35	0.31	0.10
	± 0.13	± 0.06	± 0.05	± 0.02	± 0.03	± 0.04	± 0.03
Peak 2 PCF ^b	0.27	0.30	0.04	-0.067	-0.26	-0.06	-0.11
	± 0.12	± 0.07	± 0.06	± 0.011	± 0.03	± 0.09	± 0.07

^aAll parameters are in units of phase, except the PCF which is dimensionless

^bPeak Cusping Factor

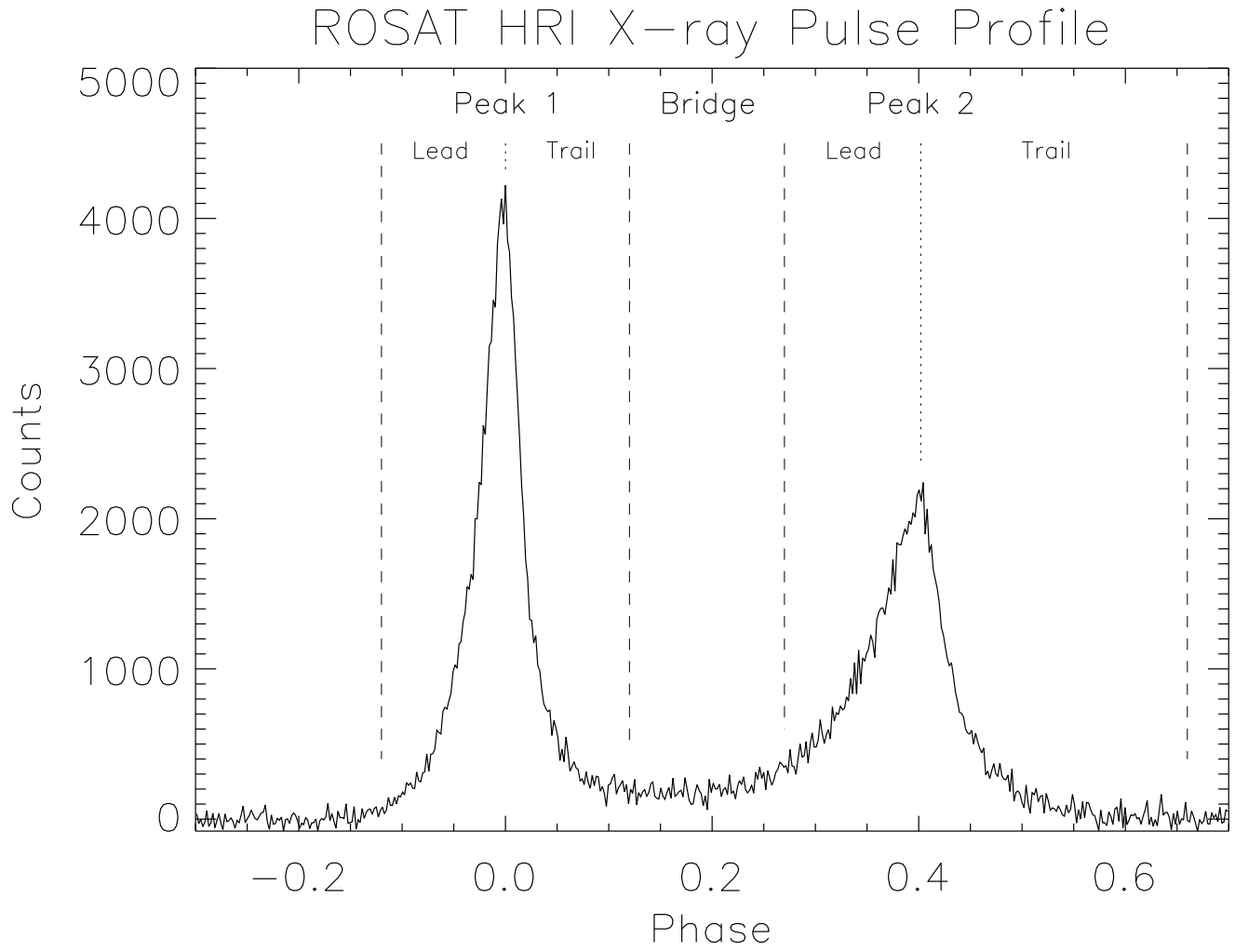


Fig. 1.— ROSAT HRI X-ray pulse profile of the Crab Nebula pulsar with $65.3\mu\text{s}$ time resolution

Figure 2(a) – J-band Pulse Profile

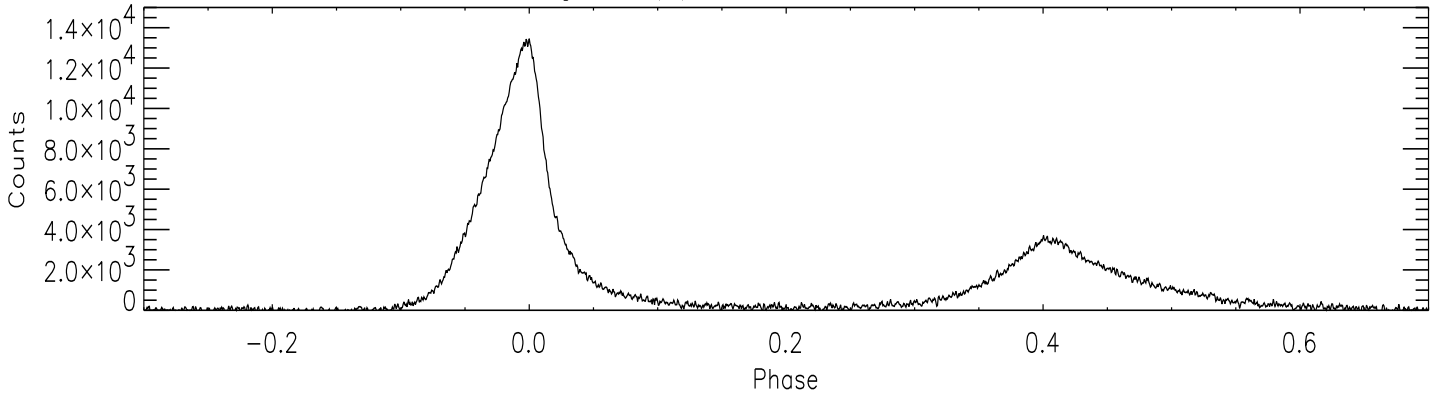


Figure 2(b) – ROSAT HRI X-ray Pulse Profile

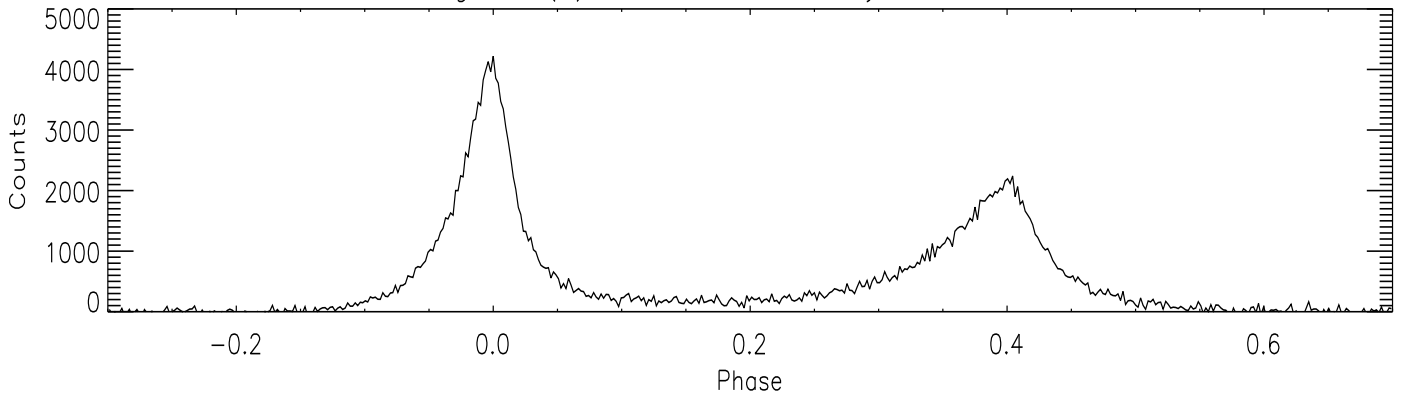


Figure 2(c) – CGRO OSSE Gamma-ray Pulse Profile

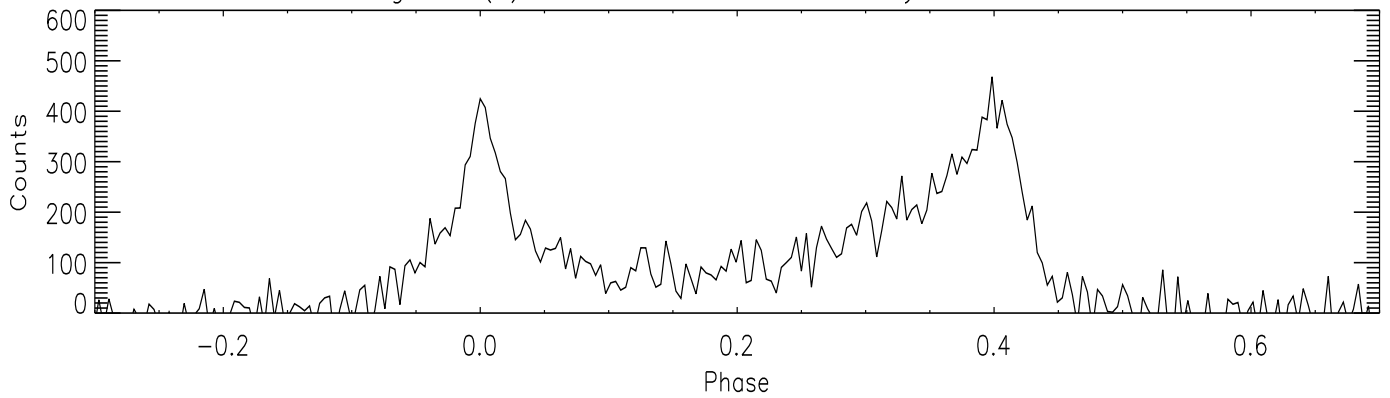


Fig. 2.— Typical pulse profiles over the IR to γ -ray energy range: (a) J-band near-infrared profile, (b) ROSAT HRI X-ray profile, (c) CGRO OSSE γ -ray profile

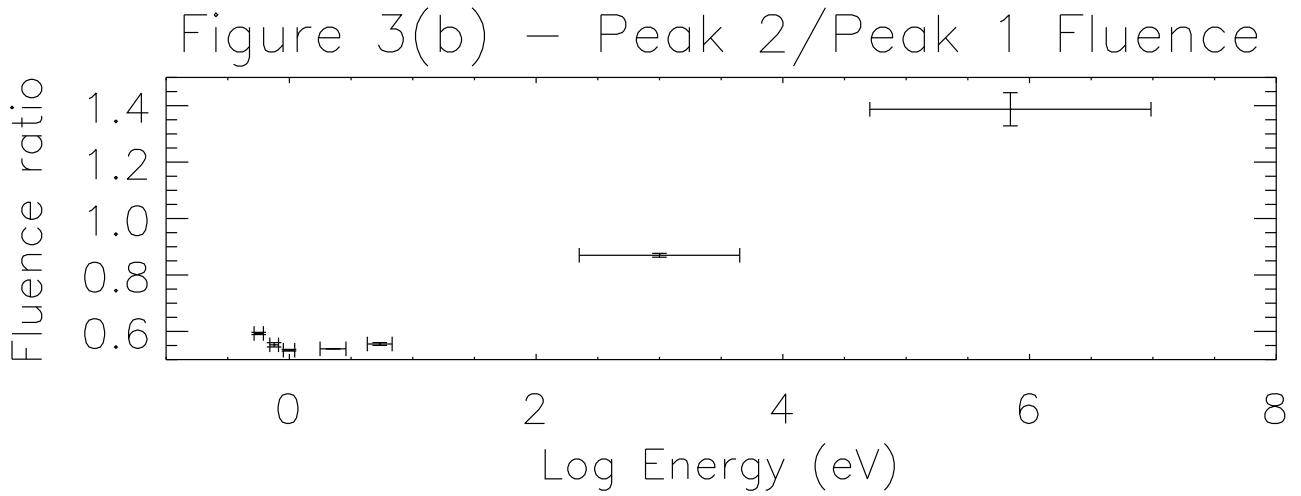
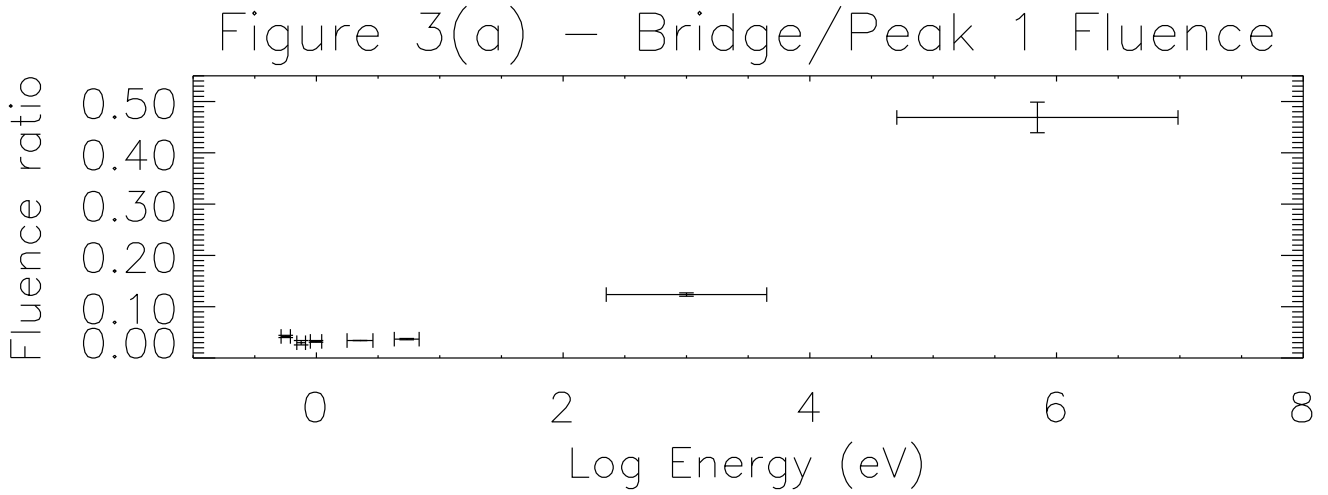


Fig. 3.— Fluence ratios of the Bridge and Peak 2 relative to Peak 1 versus energy

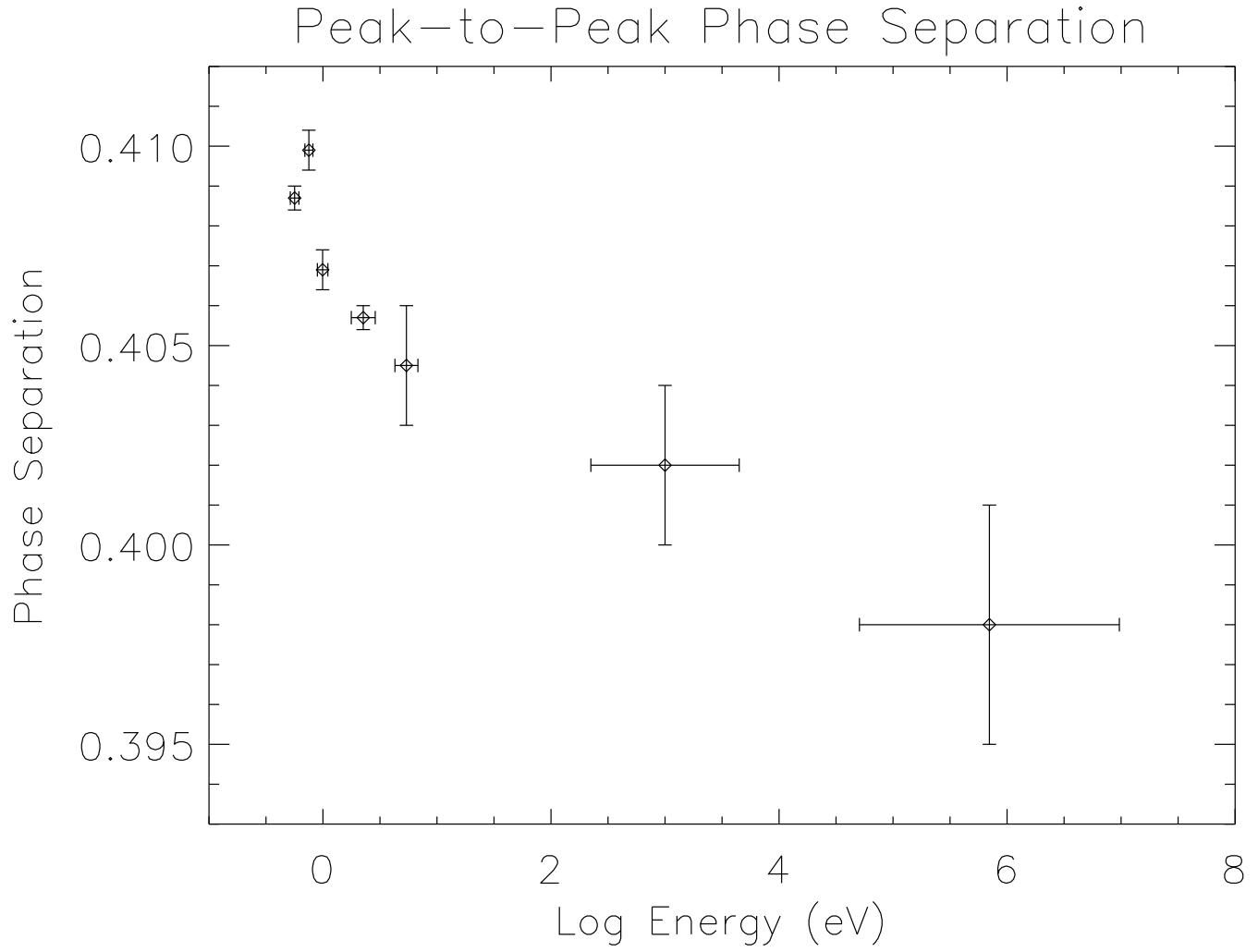


Fig. 4.— Peak-to-peak phase separation versus energy

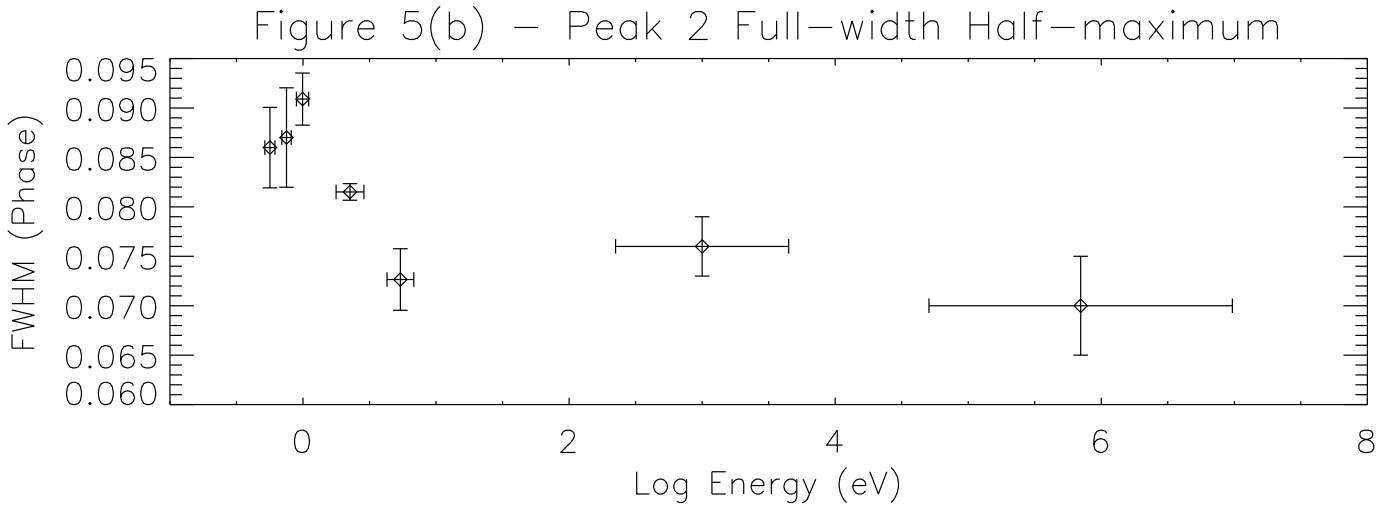
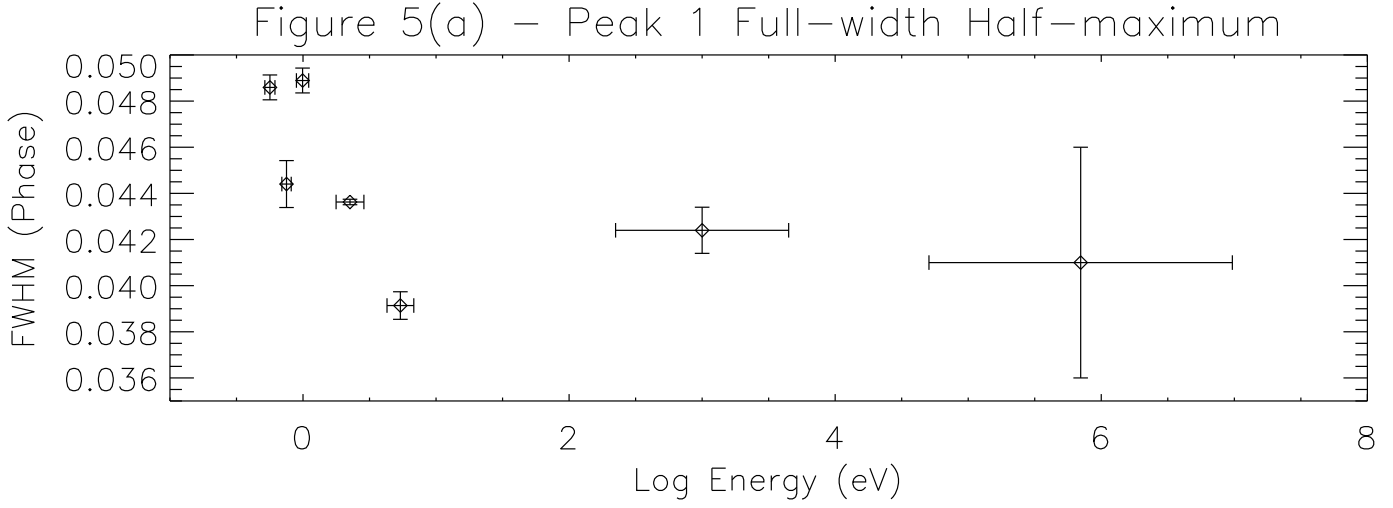


Fig. 5.— Peak full-width half-maximum versus energy for (a) Peak 1, (b) Peak 2

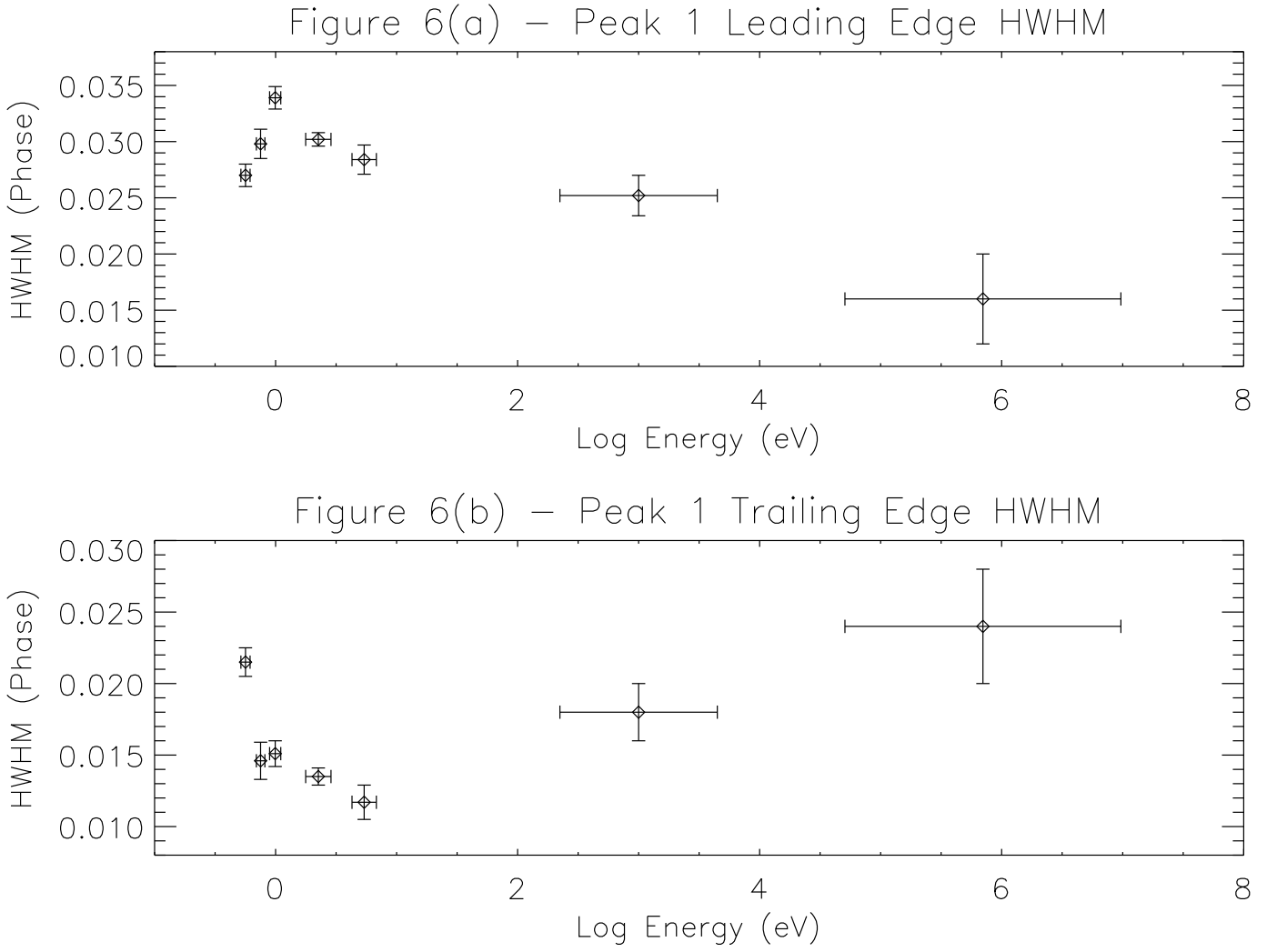


Fig. 6.— Peak half-width half-maximum versus energy for (a) Peak 1 leading edge, (b) Peak 1 trailing edge

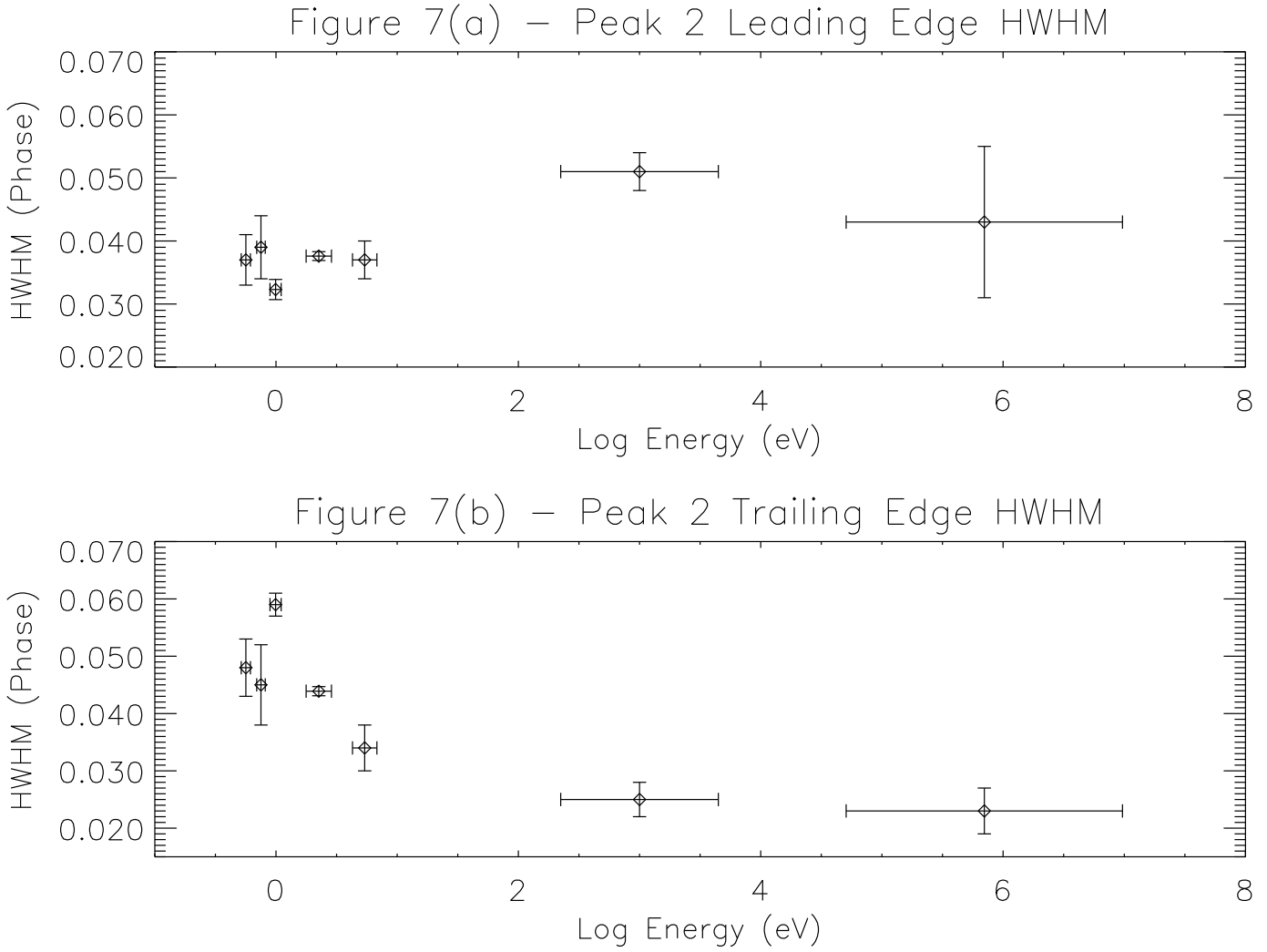


Fig. 7.— Peak half-width half-maximum versus energy for (a) Peak 2 leading edge, (b) Peak 2 trailing edge.

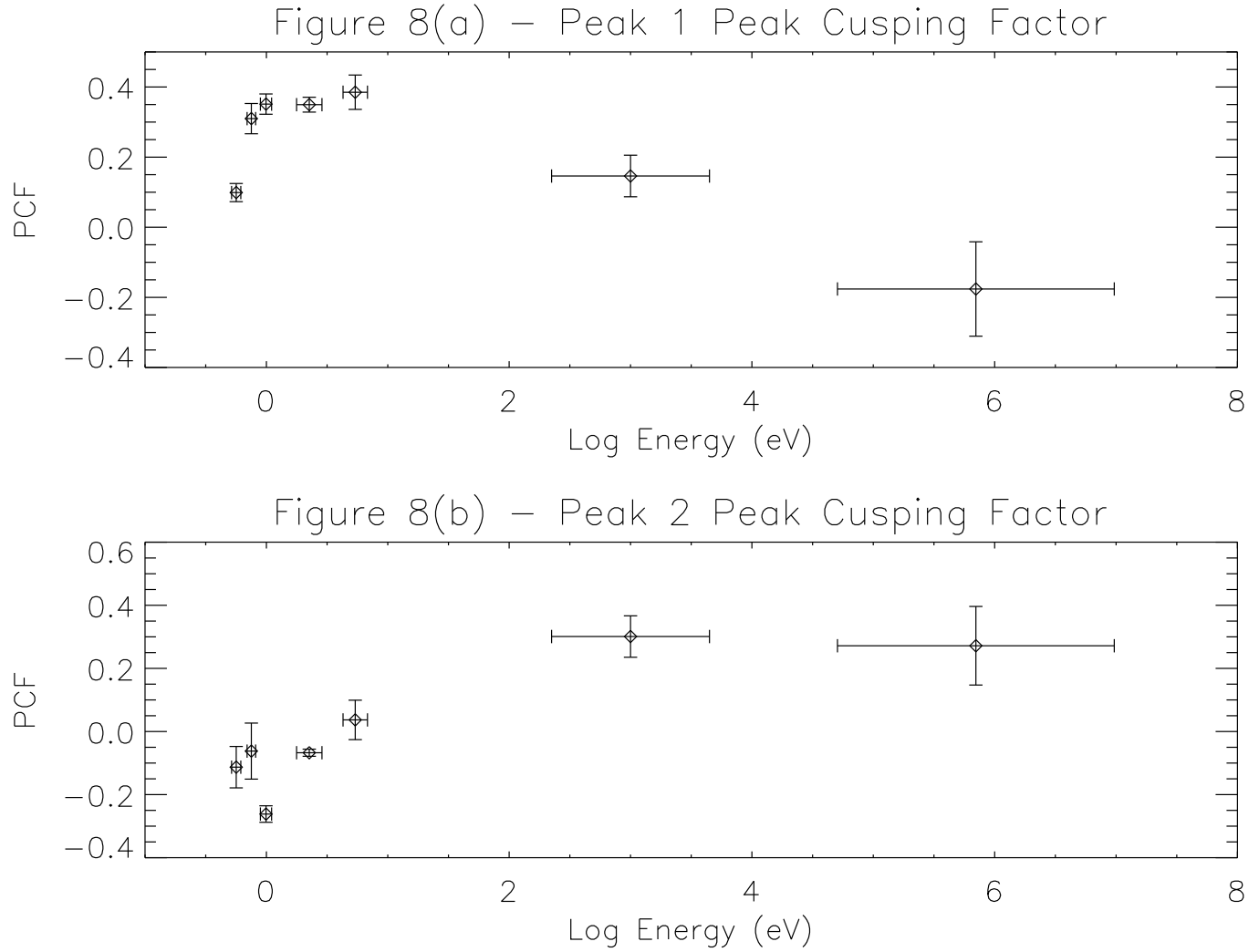


Fig. 8.— Peak cusping factor (PCF) versus energy for (a) Peak 1, (b) Peak 2

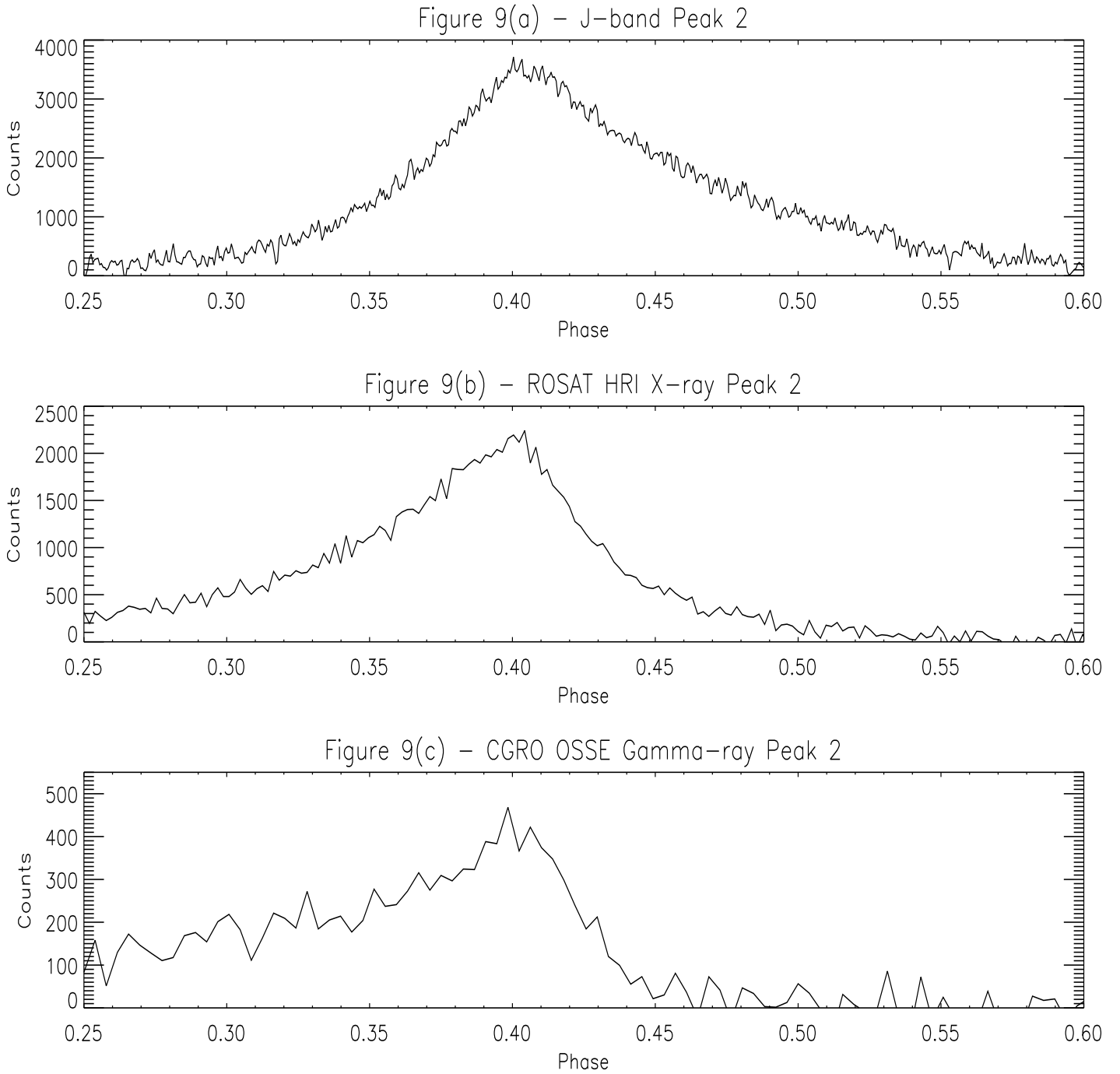


Fig. 9.— Shape of Peak 2 for (a) J-band near-infrared profile, (b) ROSAT HRI X-ray profile, (c) CGRO OSSE γ -ray profile